EFDA–JET–PR(07)12

M. Kovari, B. Crowley, S. Cox and JET EFDA contributors

Thermographic Measurement of the Emittance Plot of a Single Positive Ion Beamlet

Thermographic Measurement of the Emittance Plot of a Single Positive Ion Beamlet

M. Kovari, B. Crowley, S. Cox and JET EFDA contributors*

EURATOM-UKAEA Fusion Association, Culham Science Centre, Abingdon, OX14 3DB, UK
** See annex of M.L. Watkins et al, "Overview of JET Results ", (Proc.21st IAEA Fusion Energy Conference, Chengdu, China (2006)).*

Preprint of Paper to be submitted for publication in
Review of Scientific Instruments

"This document is intended for publication in the open literature. It is made available on the understanding that it may not be further circulated and extracts or references may not be published prior to publication of the original when applicable, or without the consent of the Publications Officer, EFDA, Culham Science Centre, Abingdon, Oxon, OX14 3DB, UK."

"Enquiries about Copyright and reproduction should be addressed to the Publications Officer, EFDA, Culham Science Centre, Abingdon, Oxon, OX14 3DB, UK."

ABSTRACT

Measurements have made of the emittance plot of a partly neutralised positive ion beamlet, using a slit, a polymer target and an infrared camera. This thermographic approach is intrinsically linear and absolute (since the properties of the target are known and approximately independent of temperature). It is sufficiently sensitive that only one short pulse is required to capture the entire range of the angular coordinate y′. Ions and neutral atoms are both detected with equal sensitivity. The measurement is unaffected by secondary electrons emitted by the target, and by electrons travelling with the positive ion beam, as both types of electron carry very little energy. No specialised electronics or beam deflection devices are required. Providing the region downstream of the mask is free of fields, the target can be several metres away from the mask, allowing good resolution in the y′ axis. The target can be as large as required.

1. INTRODUCTION

The emittance plot of a particle beam is the distribution of particle density in the xx′ or yy′ plane, where z is the beam axis, x′ = dx/dz and y′ = dy/dz [1]. It provides much more information than the emittance – a numerical quantity defined in terms of the area occupied in the emittance plot. In principle the plot can also be projected forwards or backwards to determine the size and shape of the beam at any given plane.

While most work has used electrical detectors to determine the emittance plot [2], using the principle illustrated in Fig.1, other detection methods have also been used. Various light emitting screens have been used [3], including Ce:YAG [4], and Al2O3 [5]. Guharay et al [6] used a 50μm Kapton film. The Kapton becomes darker with exposure to the beam. After a large number of identical shots the target is removed from the vessel and its transparency is measured.

This paper describes measurements of the emittance plot of a partly neutralised D^+ beam, using a slit, a polymer target and an infrared camera. The benefits of this approach are described in the abstract above.

2. MEASUREMENTS

The beam was produced by a tetrode accelerator with a standard JET ion source. The hole diameters in Grids 1 (plasma grid) to 4 (grounded grid) were 12, 13, 10 and 12mm respectively. The grid spacings are shown in Fig.2(a). The JET ion source with an accelerator is known as a “PINI” [7]. All but one of the 262 holes in the plasma grid were blocked with copper plugs. A molybdenum mask was fixed in position immediately downstream of the neutraliser. The mask had a recessed slit of nominal width 0.1mm (Fig.2(b)), and an array of recessed holes of nominal diameter 0.2mm. The final breakthrough of the holes and slit was done by laser machining [8]. The mean slit width was 0.072mm.

As the mask could not be moved, the PINI was steered up or down in steps to scan the beamlet over the slit, with one pulse taken at each position. For each pulse a series of infrared images were

taken of the target, using an infrared camera [9].

A small portion of the beamlet passed over the top of the mask. The overspill image on the target was hotter than the slit image, but sufficiently separated from it to allow the slit image to be analysed. The amount of energy passing through the array of holes was not sufficient to produce a visible infrared image.

A thermal model of the mask showed that thermal distortion greatly reduces the slit width if the pulse length ~ 100ms. If the parallel-sided recess was replaced by a V-shaped chamfer this problem would be greatly reduced. Note that in either case the recess or chamfer should be on the upstream side. This is the opposite of the approach normally used to prevent scattering. The recess used was wide enough that any scattered particles will land well away from the target.

The target was Kapton XC, 40μm thick. This is a black, carbon-loaded, electrically conductive polyimide, thermally durable to 325ºC in oxygen-free environments10. The carbon is present throughout the bulk of the film, so it cannot rub or flake off. Non-loaded Kapton is translucent, both in the visible and infrared. The carbon makes the film opaque, and prevents charging from the beam.

The timescale for heat to spread through the thickness of the target is of the order of (target thickness)2/thermal diffusivity = 0.02s. The thermal images used for analysis were taken about 50 ms after the end of the pulse, long enough for the temperature to be uniform through the thickness of the target, but short enough that very little heat spreads transversely.

The emissivity of Kapton XC was measured in air. Linear fits to the emissivity are 0.95−0.0007Q and 0.94 - 0.0005Q for the matt and shiny sides respectively, where Q is the temperature in ºC.

3. DATA COLLECTION AND ANALYSIS

The last image before the pulse was subtracted from the image taken about 50ms after the end of the pulse, giving a temperature change image (Fig.3). A set of lines was drawn on the image, parallel to each other and to the axis of the slit image. The mean temperature rise along each line was calculated. Each pulse corresponds to one value of y. Each line corresponds to one value of y′. The differential power at the mask is given by

$$\frac{d^2P}{dydy'} \Delta T \frac{c\rho d}{t} \cdot \frac{Ld_{mt}}{\delta}, \qquad (1)$$

where P is the power at the mask; y and y’ are shown in Fig. 1; ΔT is the temperature rise of the target, averaged along one line; c is the specific heat capacity of target; ρ is the density of target; d is the thickness of target; t is the pulse length; L is the length of a line on the image; dmt is the distance from mask to target; and δ is the width of the slit in the mask.

The emittance plot shows $d^2P/dydy'$ against y and y′.These measurements give the emittance plot at the mask. Assuming the region is field-free, the emittance plot at any other plane can be calculated.

4. RESOLUTION

The emittance diagram is most usefully plotted at Grid 4, since beam simulations are likely to end there. Consequently it is important to estimate the achievable spatial and angular resolution at Grid 4.

Figure 4 illustrates the effect that the finite spatial resolution of the IR camera has on the resolution of the emittance plot at Grid 4. The two lines represent extreme particle paths that land on points of the target that are too close to be distinguished. The angle between the paths represents the angular resolution, and the separation of the paths at Grid 4 represents the spatial resolution. Figure 5 illustrates the effects of slit width. The two lines represent extreme particle paths that cannot be distinguished because they land in the same place on the target.

Combining these two effects, the net spatial resolution Δy at grid 4 is

$$\Delta y = \sqrt{\left(\delta \cdot \frac{d_{mt} + d_{gm}}{d_{mt}}\right)^2 + \left(p \ \frac{d_{gm}}{d_{mt}}\right)^2} \tag{2}$$

and the angular resolution $\Delta y'$ is

$$\Delta y = \sqrt{\left(\frac{\delta}{d_{mt}}\right)^2 + \left(\frac{p}{d_{mt}}\right)^2}, \tag{3}$$

where p is the spatial resolution of the IR camera at the target; d_{gm} is the distance from grid 4 to mask, and d_{mt} and d are defined above.

These formulae need to be modified if the target is not normal to the beam. Estimates using these formulae are Δy = 0.8 mm and $\Delta y'$ = 0.4mrad, but it is not possible to confirm these using the measured results. The beam was not scanned over the slit in small enough steps to cover the emittance plot in sufficient detail.

When using a pepper-pot the diameter of the image of a pinhole must be calculated to ensure that the separate pinhole images do not overlap. The geometrical image of the aperture in Grid 4 is the upper limit. The angular spread of the beamlet determines whether this image is fully illuminated. Consequently the image on the target of a pinhole on the beamlet axis is given by the smaller of the two quantities,

$$a = \phi_{beamlet} \cdot \frac{d_{mt}}{d_{gm}}, \ and \ b = \theta_c \cdot d_{mt}, \tag{4}$$

where $\phi_{beamlet}$ is the diameter of the beamlet at Grid 4; and θ_c is the maximum angle of convergence of the particles reaching the mask. (Whether this is the same as the overall beamlet divergence angle depends on the shape of the emittance plot.)

RESULTS

The emittance plots at the mask and extrapolated to Grid 4 are shown below. The origins of the y

and y′ scales are arbitrary. It is not possible to calculate the emittance, as much of the emittance plot is missing because it was not possible to scan the beamlet sufficiently far up or down.

CONCLUSIONS

The thermography technique for measurement of emittance plots was successful, but in the angular coordinate (y′) measured at Grid 4 the sampling interval was too large and the extent of coverage was insufficient. Several improvements are suggested:

1. The mask should be bigger to prevent overspill.
2. The slit should be chamfered rather than recessed to minimise thermal distortion.
3. The mask should be as close as possible to the accelerator to improve resolution in y. To ensure adequate sampling the mask must be stepped in fractions of a millimetre, right out to the edge of the beam.
4. An aperture with no offset aperture steering should be used, to guarantee symmetry. A second aperture with steering, well separated from the first, could be used for comparison.

ACKNOWLEDGEMENTS

This work is dedicated to our colleague Stephen Cox whose tragic death occurred whilst this work was in progress. M. Kovari and B. Crowley would like to thank F. Long, M. Barnard, R. Robins and T. Jones. This work has been conducted under the European Fusion Development Agreement and is funded partly by EURATOM and by the UK Engineering and Physical Science Research Council.

[1]. J. D. Lawson, The Physics of Charged-Particle Beams, 2nd ed., Clarendon (1988).

[2]. C. Lejeune and J. Aubert, Advances in Electronics and Electron Physics, Supplement **13A**, 159 (1980).

[3]. J. G. Wang, D. X. Wang, M. Reiser, Nuclear Instruments and Methods in Physics Research, A, **A307**, 190 (1991).

[4]. L. Catani, E. Chiadroni, A. Cianchi, S. Tazzari, M. Boscolo, M. Castellano, G. Di Pirro, M. Farrario, V. Fusco, D. Filipetto, L. Palumbo, C. Vaccarezza, C. Vicario, C. Ronsivalle, Rev. Sci. Instrum. **77**, 093301 (2006).

[5]. T. Hoffmann, W. Barth, P. Forck, A. Peters, P. Strehl, D.A. Liakin, 9th Beam Instrumentation Workshop 2000, AIP Conference Proceedings, **546**, 432 (2000).

[6]. S. K. Guharay, K. Tsumori, M. Hamabe, Y. Takeiri, O. Kaneko and T. Kuroda, Rev. Sci. Instrum. **67**, 2534 (1996).

[7]. G. Duesing, H. Altmann, H. Falter, A. Goede, R. Haange, R.S. Hemsworth, P. Kupschus, D. Stork and E. Thompson, Fusion Technology **11**, 163 (1987)

[8]. UK Laser Micromachining Centre, www.uk-lmc.co.uk

[9]. Agema Thermovision 550, FLIR Systems, +44(0)1732-220-011, www.flir.com

[10]. www2.dupont.com

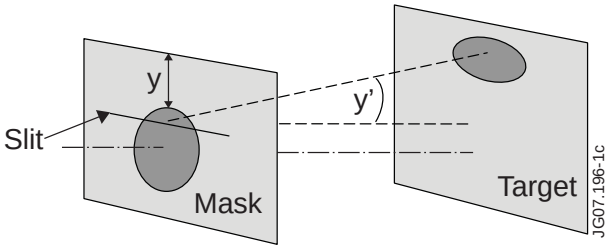

Figure 1: The principle of measurement of the emittance plot.

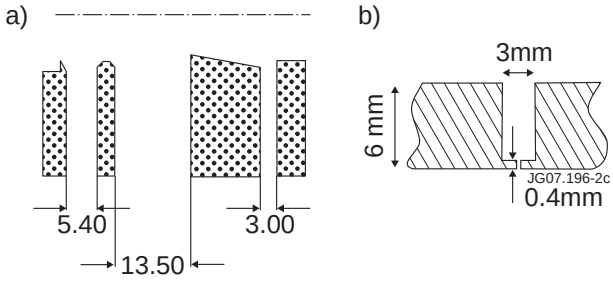

Figure 2: (a) cross-section of grid, with half of the aperture. (b) cross-section of slit in mask.

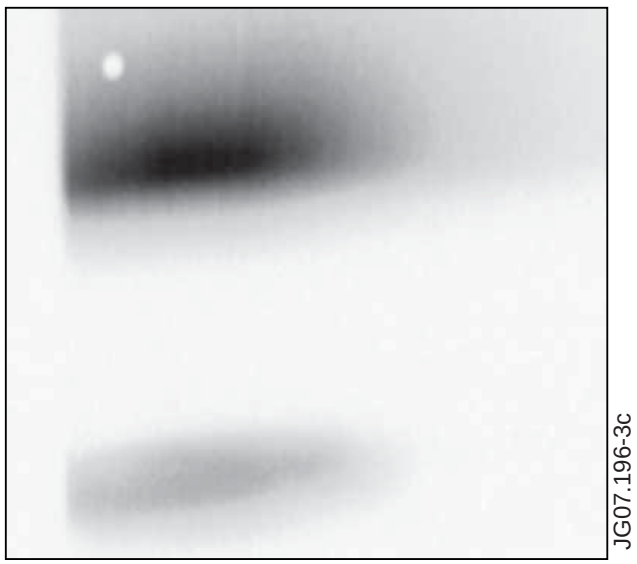

Figure 3: Typical infrared image, showing overspill (top) and slit image (bottom)

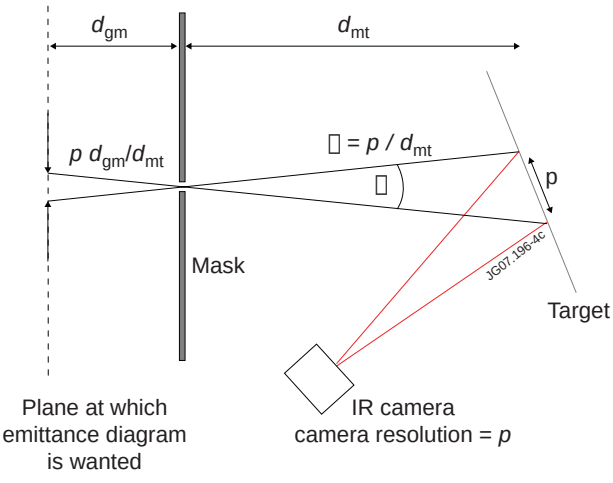

Figure 4: The effect of the resolution of the IR camera.

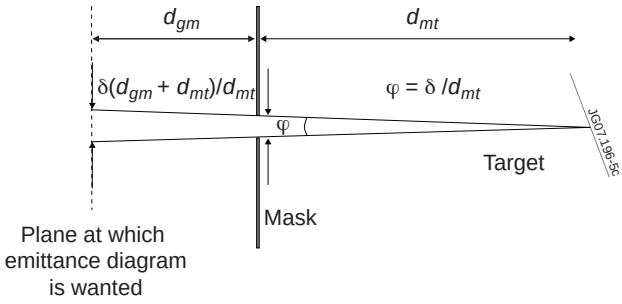

Figure 5: The effect of slit width

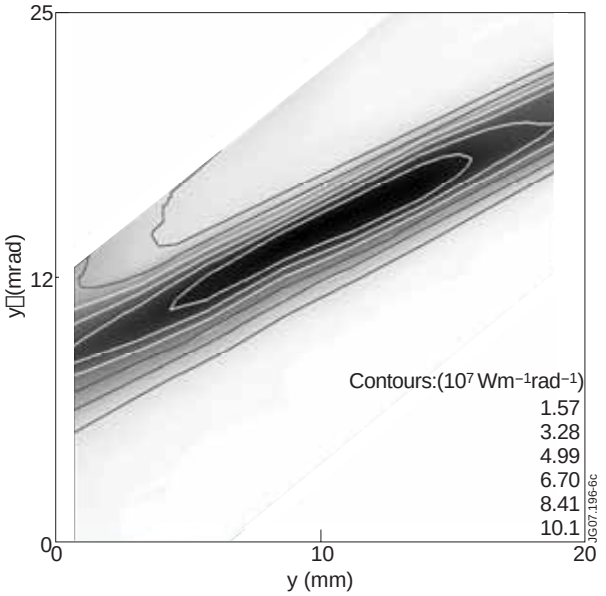

Figure 6: Emittance plot at mask, 108 kV, pulse length 37 ms, 122 mA